High Power Laser Science and Engineering, (2019), Vol. 7, e32, 5 pages.

doi:10.1017/hpl.2019.19

High-repetition-rate, high-peak-power 1450 nm laser source based on optical parametric chirped pulse amplification

Pengfei Wang[1,2,†], Beijie Shao[1,2,†], Hongpeng Su[1,2], Xinlin Lv[1,2], Yanyan Li[1], Yujie Peng[1], and Yuxin Leng[1]

[1]*State Key Laboratory of High Field Laser Physics, Shanghai Institute of Optics and Fine Mechanics, Chinese Academy of Sciences, Shanghai 201800, China*

[2]*Center of Materials Science and Optoelectronics Engineering, University of Chinese Academy of Sciences, Beijing 100049, China*

(Received 20 September 2018; revised 17 March 2019; accepted 8 April 2019)

Abstract

We present a high-peak-power, near-infrared laser system based on optical parametric chirped pulse amplification pumped by a home-built picosecond pumping laser, which can generate over 40 mJ energy at 1450 nm center wavelength and operate at 100 Hz repetition rate. Subsequently, the chirped laser pulses are compressed down to 60 fs with 26.5 mJ energy, corresponding to a peak power of 0.44 TW. This high-energy, long-wavelength laser source is highly suitable for driving various nonlinear optical phenomena, such as high-order harmonic generation and high-flux coherent extreme ultraviolet/soft X-ray radiation.

Keywords: infrared lasers; nonlinear optics; ultrafast lasers

1. Introduction

High-order harmonic generation (HHG) has been attracting increasing attention due to its excellent properties, such as high peak intensity and brightness, full coherence, wide tunability, and creation of isolated attosecond pulses[1, 2]. In particular, high-energy, few-cycle infrared pulses have a tremendous impact on HHG features in many experiments, owing to the high ponderomotive energy $U_p \propto I\lambda^2$ at moderate intensity levels and a longer carrier wavelength λ. For example, the HHG cut-off energy scales as λ^2[3], but the HHG efficiency scales approximately as λ^{-5}–λ^{-6} in the single-atom gas[4, 5]. Therefore, with the aim of extending the HHG cut-off energy with high efficiency, there is increasing interest in the development of high-peak-power, high-repetition-rate carrier-envelope phase (CEP)-stabilized near-infrared laser systems. Optical parametric amplification (OPA) and optical parametric chirped pulse amplification (OPCPA) are major methods to directly deliver high-peak-power infrared pulses with multi-cycle pulse durations to that with near single-cycle pulse durations.

Correspondence to: Y. Li, Y. Peng, and Y. Leng, No. 390 Qinghe Road, Jiading District, Shanghai 201800, China. Email: yyli@siom.ac.cn (Y. Li), yjpeng@siom.ac.cn (Y. Peng), lengyuxin@mail.siom.sc.cn (Y. Leng)

[†]These authors contributed equally to this work.

Using OPA, near-infrared laser pulses with multi-millijoule energy have been generated by various methods. Takahashi *et al.* reported a 1.4 μm laser system running at 10 Hz repetition rate with 7 mJ energy and 40 fs duration based on OPA, and employed it successfully to generate soft X-ray harmonics[6]. Bruno *et al.* used OPA to generate pulses with 10 mJ energy and 5-cycle duration at 1.8 μm[7] and compressed the pulse duration to 2-cycle via a hollow-core fiber (HCF) post-compression system[8]. For few-cycle laser pulse generation, variform OPAs also can be used directly. For instance, a new method called frequency-domain OPA (FOPA) has been reported to generate laser pulses with 1.43 mJ energy and 11.9 fs duration at 1.8 μm and running at 100 Hz repetition rate[9, 10]. With dual-chirped OPA (DC-OPA), scientists at RIKEN obtained infrared pulses over 100 mJ in the wavelength range 1–2 μm[11] and 0.3 TW peak power mid-infrared pulses near 3.3 μm[12] in 2018. Another method is to employ periodically poled crystals to obtain broadband gain in a quasi-phase-matched (QPM) OPA. With this method, 0.74 mJ/15.7 fs[13] and 1.2 mJ/10.5 fs pulses[14] at 2.1 μm have been reported. In addition, some researchers have used self-phase modulation (SPM) to broaden the pulse spectral bandwidth and then employed chirped mirrors or anomalous dispersion materials to compensate the pulse dispersion

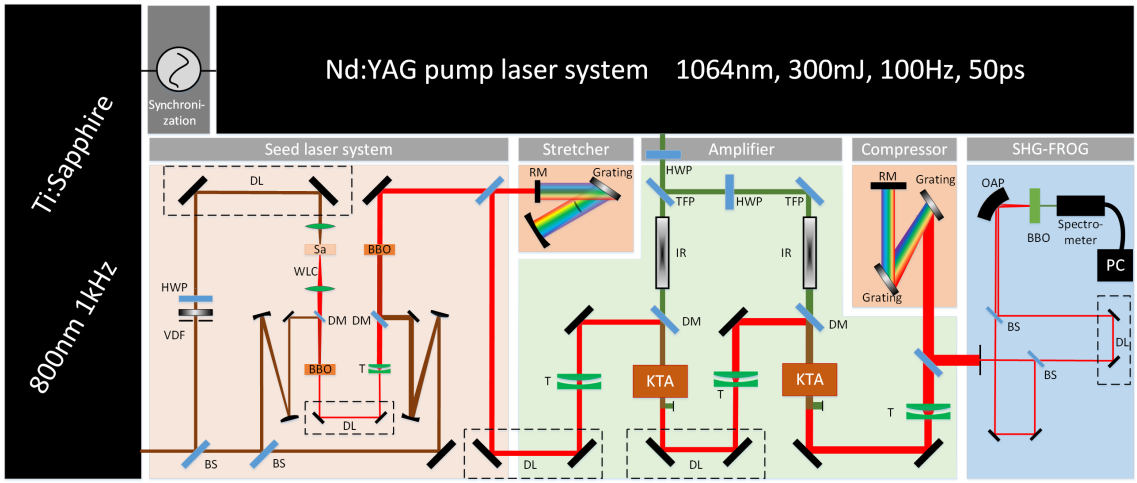

Figure 1. Schematic of the OPCPA setup. DL, delay line; TFP, thin film polarizer at 1064 nm; DM, dichroic mirror; BS, beam splitter; HWP, half-wave plate; WLC, white-light continuum; Sa, sapphire; RM, roof mirror; IR, image relay; OAP, off-axis parabolic mirror; VDF, variable density filter; T, telescope; PC, computer.

to generate few-cycle pulses. Lasers with 2.5 mJ/22 fs at 3.2 μm[15] and 2.6 mJ/21.5 fs at 4.0 μm[16] have been reported. Therefore, OPA is a relatively simple method to generate infrared pulses with multi-millijoule energy and multi-cycle pulse duration, but its output capability is greatly restricted by the pump energy, and it is not suitable for generating energies of tens of millijoules or higher.

With the benefits brought by the rapid development of high-energy solid-state laser systems[17, 18], the pump energy for OPCPA has the capability to reach hundreds, or even thousands, of millijoules. For instance, 8 mJ/80 fs pulses at 3.9 μm using 250 mJ pump energy based on KTA crystals[19] and 3 mJ/11.4 fs pulses at 1.7 μm (0.26 TW peak power) with 18 mJ pump energy based on BBO crystals[20] have been reported. Mitrofanov *et al.* also reported a 3.9 μm laser system with 35 mJ energy and 80 fs duration (0.44 TW) running at 20 Hz[21, 22] in 2017 – the system employed KTA crystals and up to 1 J pump energy. Moreover, Qian *et al.* reported a quasi-parametric chirped pulse amplification (QPCPA) method[23], which greatly increases the conversion efficiency in the parametric process, and they are developing a mid-infrared laser operating at 2.2 μm at the 100 TW level[24].

In this paper, we demonstrate a high-peak-power 1450 nm laser system based on OPCPA, which can generate pulses with greater than 40 mJ energy running at 100 Hz. The chirped laser pulses are then compressed down to 60 fs with 26.5 mJ energy, which indicates a peak power of 0.44 TW. This high-energy, high-peak-power near-infrared laser source is suitable for generating high-flux ultrafast soft X-ray pulses by driving HHG and for generating sub-100 fs hard X-ray pulses by driving plasma emission.

2. Laser schematic

The high-peak-power laser system is based on an OPCPA scheme which includes a 1 kHz Ti:sapphire chirped pulse amplification (CPA) laser, a BBO-based OPA seed laser system, an Öffner stretcher, an OPCPA amplifier, a home-built Nd:YAG pump laser system, a two-grating compressor and a home-built second-harmonic generation frequency-resolved optical gating (SHG-FROG) measurement device, as shown in Figure 1.

In the system, the commercial Ti:sapphire CPA laser (Astrella, Coherent Inc.) provides a portion of 40 fs, 3.0 mJ pulses at 800 nm with a repetition rate of 1 kHz as the driving source of the system. The 800 nm pulses are used to pump the BBO-based OPA which is the seed of the OPCPA system. The timing clock is obtained from the Ti:sapphire CPA laser. Briefly, a small portion of the pump is used to generate a white-light continuum (WLC) in a sapphire plate. Then the signal from the WLC is amplified in the following parametric processes. Owing to the high nonlinearity and broad phase-matching bandwidth, BBO crystals (cut at $\theta = 27.2°$ for type-II phase-matching) are selected to amplify the signal.

For the OPA system, the output amplified pulse energy is 190 μJ at 1.45 μm with an energy fluctuation of less than 1% (rms). This 1.45 μm laser pulse is injected into the OPCPA system as the seed. To achieve efficient amplification, the seed pulse duration is stretched to 50 ps (full-width at half-maximum, FWHM) to match that of the pump. Here, a conventional Öffner-type stretcher based on a 600 grooves/mm gold-coated grating is employed.

The pump of the OPCPA system also comes from a home-built picosecond laser source based on a master oscillator power amplifier (MOPA) configuration, which contains a home-built Nd:YVO_4 mode-locked oscillator, a regenerative

https://doi.org/10.1017/hpl.2019.19 Published online by Cambridge University Press

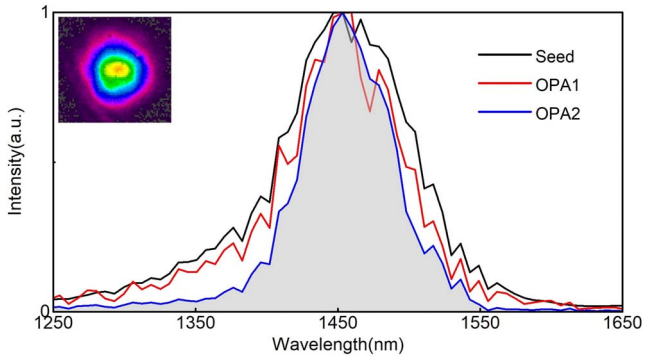

Figure 2. Spectrum evolution through the OPCPA system. Insert, near-field beam profile after the second KTA crystal, as measured by a pyroelectric thermal camera (PyroCAM) with a spatial resolution of 80 μm.

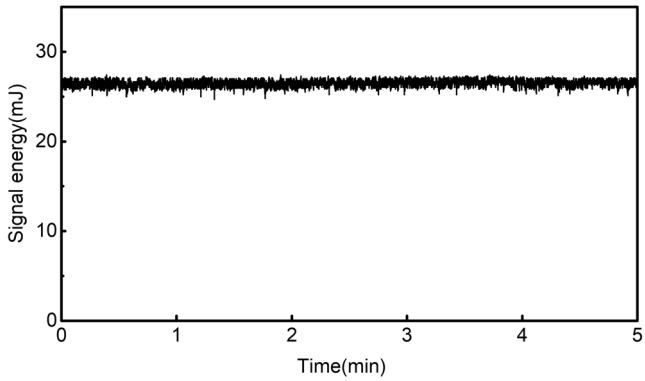

Figure 3. Energy fluctuation of compressed pulses at 1450 nm.

amplifier based on a laser diode pumped Nd:YAG crystal, and two double-pass Nd:YAG power amplifiers[25]. The pump system can deliver 1064 nm laser pulses with 316.5 mJ energy and 50 ps pulse duration running at 100 Hz repetition rate. The flat-top beam profile and 0.53% (rms) energy fluctuation make it suitable for pumping the OPCPA.

The main issue to be settled for the OPCPA system is time synchronization between the seed and pump pulses. Here, to achieve perfect temporal synchronization, a home-built oscillator for the pump system is designed to operate at 80 MHz, which is the same as that of the commercial 800 nm oscillator (VITARA, Coherent Inc.). Furthermore, the VITARA is equipped with a synchronization accessory (SLAP, Coherent Inc.) with which its oscillator can be synchronized with an external radio frequency (RF) source. A fraction of the pulses from the home-built Nd:YVO_4 mode-locked laser are utilized and converted as the master signal by a photo-diode. The synchronization accessory accepts the master signal as the trigger and automatically adjusts the cavity length of the VITARA to achieve precise frequency synchronization between the two oscillators. Using the synchronization accessory, the timing jitter between the pump and signal pulses is controlled to about 300 fs.

The energy of the stretched seed pulse is 60 μJ with 50 ps duration. The beam size of the pulse is expanded to 4 mm diameter by a telescope system. The seed pulse is then injected into the first 10 mm thick KTA crystal, cut at $\theta = 40.8°$ in the x–z plane for type-II phase-matching. At the same time, part of the pump pulse also arrives at the first KTA crystal with a 60 mJ energy and a 4 mm beam diameter with a flat-top profile. The pump, signal and/or idler beams are combined and separated before and after the KTA crystal by pairs of dichroic mirrors (highly reflective at 1064 nm, anti-reflective around 1450 nm and 4000 nm). The relative delay of the signal and pump pulses can be adjusted by a delay line (DL), as shown in Figure 1. After the first OPA stage, the 1.45 μm seed pulse has a 4.9 mJ energy and is retained for further amplification (the spectrum is plotted as the red curve in Figure 2). At the same time, the idler pulse at 3.9 μm and the residual pump pulse are rejected by two other similar dichroic mirrors (highly reflective around 4000 nm, anti-reflective around 1450 nm) to prevent double seeding of the second amplification stage.

For the second OPA process, the beam sizes of both the pump and signal pulse are enlarged to 6 mm to prevent the KTA crystal and the dichroic mirrors from being damaged by the high peak power of the pump pulse. The second KTA crystal is also cut for type-II phase-matching at $\theta = 40.8°$ in the
x–z plane and with 10 mm thickness. Here, restricted by the damage threshold of the dichroic mirrors, only 220 mJ pump energy is employed to amplify the signal pulse. After the second OPA process, pulses with 42 mJ energy at 1.45 μm and 14.5 mJ energy at 3.9 μm are achieved. The signal spectrum after the second amplifier is only slightly narrower than the seed spectrum, as shown in Figure 2.

The pulse with 42 mJ energy at 1.45 μm is sent to a two-grating compressor. The compressor consists of two gratings which are the same as that used in the stretcher (600 grooves/mm). This is used to compensate the dispersion introduced in the stretcher. Up to 26.5 mJ energy with 1.12% (rms) energy fluctuation (shown in Figure 3) is obtained after the compressor with a total efficiency of 73%.

Temporal characterization of the infrared pulse at 1.45 μm generated from OPCPA is measured by a home-built SHG-FROG setup employing a 200 μm-thick BBO crystal. By optimizing the grating angles and separation distance in the compressor, the shortest duration obtained at 1.45 μm is 60 ± 1 fs (<0.46% rms error over a 256 × 256 calculation grid) at FWHM, which is within 6% of the Fourier-transform limit (56.7 ± 1 fs). The uncertainty on the latter values arises from the limited dynamic range of the FROG measurement and the inevitable choice of a spectral threshold to distinguish the signal from background and noise. Temporal and spectral characterizations of the OPCPA output pulse, along with the corresponding spectrum and phase retrieved from the SHG-FROG measurement results are shown in

https://doi.org/10.1017/hpl.2019.19 Published online by Cambridge University Press

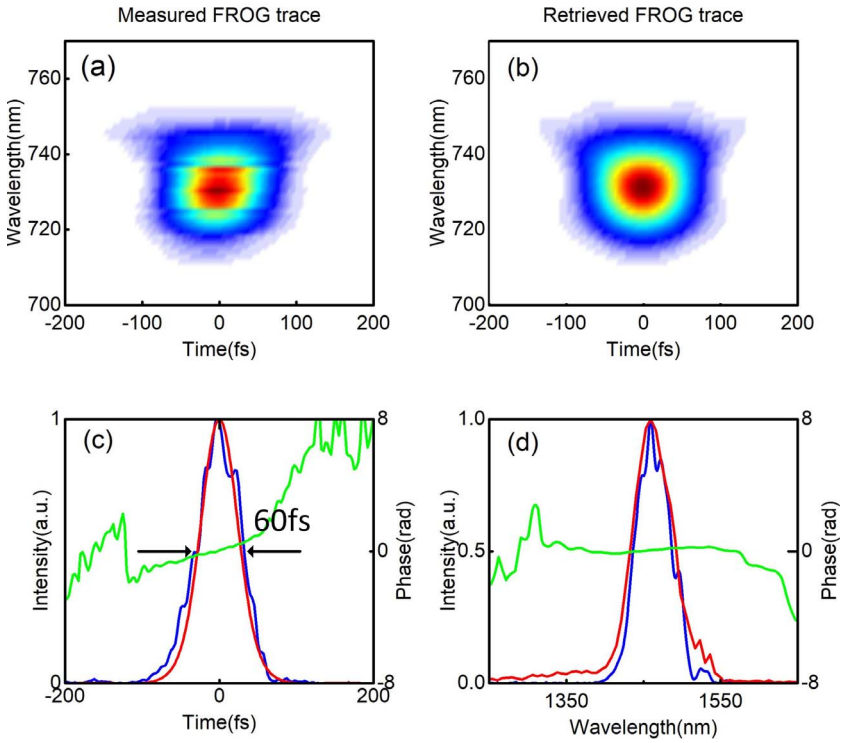

Figure 4. Temporal characterization of the compressed pulse. (a) Measured and (b) retrieved SHG-FROG traces; (c) reconstructed pulse envelope (blue), which is 60 fs (FWHM), phase (green) and its TL pulse (red); (d) reconstructed spectrum (blue), phase (green) and measured spectrum (red) obtained by a near-infrared spectrometer (NIR-Quest from Ocean Optics).

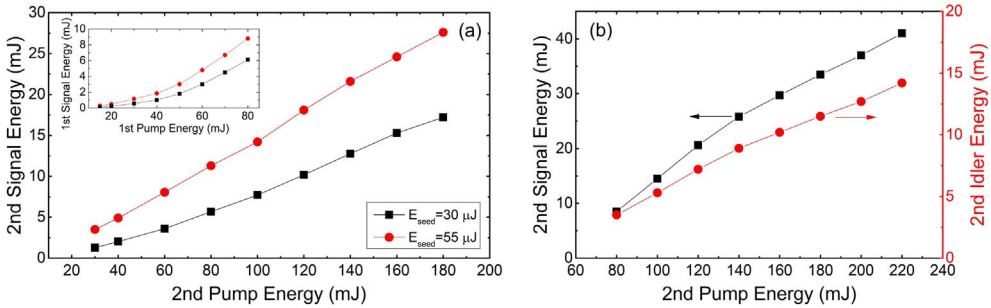

Figure 5. (a) Amplified signal energy as a function of pump energy (seed energy fixed) of the first (insert) and the second OPA stages. (Black) Seed energy fixed at 30 μJ. (Red) Seed energy fixed at 55 μJ. (b) Amplified signal (black dots) and idler (red dots) energies as functions of pump energy in the second OPA stage (the energy of the first amplified signal is fixed at 4.9 mJ).

Figure 4. Figures 4(a) and 4(b) are the measured and retrieved traces by the SHG-FROG, respectively. Figure 4(c) shows the reconstructed pulse (blue), phase (green) and its transform-limited (TL) pulse (red), which indicates the compressed pulse duration is only 60 fs. Figure 4(d) shows the reconstructed spectrum (blue), measured spectrum (red) and phase (green).

3. Discussion

Furthermore, we characterized the gain in the high-energy second OPA stage as a function of the seed and pump energies, as shown in Figure 5. The pump energy of the second OPA process varies from 30 mJ to 180 mJ with seed energies of 30 μJ and 55 μJ, respectively. We can see that there exists a linear dependence between the amplified signal energy and the pump energy. But when the pump energy is below 40 mJ, the gain of the first OPA process is very low and increases slowly with the pump energy, as shown in the insert of Figure 5(a). With 55 μJ seed energy, the amplified 1.45 μm signal energy of the second OPA process increases from 3.5 mJ (30 mJ pump energy) to 27.6 mJ (180 mJ pump enrgy). However, with 30 μJ seed energy and the same pump energy, the maximum signal energy of the second OPA process is only 17.2 mJ. We have also characterized the amplified 1.45 μm signal energy of the second OPA process while keeping the energy of the first amplified signal fixed at

https://doi.org/10.1017/hpl.2019.19 Published online by Cambridge University Press

4.9 mJ and varying the second OPA pump energy from 80 mJ to 220 mJ, as shown in Figure 5(b). The linear dependence between the energies of the pump and signal pulse indicates that the second OPA stage has not yet reached saturation. If a higher pump energy can be employed successfully for the second OPA stage, a higher amplified pulse energy at 1.45 μm would be obtained from the OPCPA system.

It is worth mentioning that there are several limitations restricting the output energy in this experiment. The first is the limited damage threshold of the coatings on the dichroic mirrors. To prevent damage in the system, only 220 mJ pump energy is used in the second amplification process, which therefore does not reach its saturation state. The second is the low transmission of some of the optical elements used in the system, such as several uncoated CaF_2 lenses (each one has 7% absorption and reflection losses), and the low transmission of the nonlinear crystals. These uncoated optical elements cause poor efficiency (>20% losses) of the whole OPCPA system. Therefore, several methods used to improve the output capability would be effective, such as using higher-damage-threshold dichroic mirrors and replacing optical elements with those of high transmittance.

4. Conclusion

To sum up, we report a 100 Hz, high-peak-power infrared laser system employing a two-stage collinear OPCPA. Pulses with over 40 mJ energy at 1450 nm are generated, and the pulses are compressed down to 60 fs with 26.5 mJ energy, indicating a peak power of 0.44 TW. This high-energy infrared laser source is suitable for driving various nonlinear optical phenomena such as high harmonic generation to obtain high-flux ultrafast soft X-ray pulses, the generation of sub-100 fs hard X-ray pulses using laser-driven plasma emission from a copper target, and the generation of intense single-cycle THz pulses through plasma emission driven in a two-color laser field.

Acknowledgements

This work is funded by the Strategic Priority Research Program of the Chinese Academy of Sciences (No. XDB1603), National Natural Science Foundation of China (Nos.11127901, 61521093 and 61635012), International S&T Cooperation Program of China (No. 2016YFE0119300), Program of Shanghai Academic/Technology Research Leader (No. 18XD1404200) and Shanghai Municipal Science and Technology Major Project (No. 2017SHZDZX02).

References

1. T. Sekikawa, A. Kosuge, T. Kanai, and S. Watanabe, Nature **432**, 605 (2004).
2. G. Sansone, E. Benedetti, F. Calegari, C. Vozzi, L. Avaldi, R. Flammini, L. Poletto, P. Villoresi, C. Altucci, R. Velotta, S. Stagira, S. De Silvestri, and M. Nisoli, Science **314**, 443 (2006).
3. P. B. Corkum, Phys. Rev. Lett. **71**, 1994 (1993).
4. N. Thiré, S. Beaulieu, V. Cardin, A. Laramée, V. Wanie, B. E. Schmidt, and F. Légaré, Phys. Rev. Lett. **98**, 013901 (2007).
5. P. Colosimo, G. Doumy, C. I. Blaga, J. Wheeler, C. Hauri, F. Catoire, J. Tate, R. Chirla, A. M. March, G. G. Paulus, H. G. Muller, P. Agostini, and L. F. DiMauro, Nat. Phys. **4**, 386 (2008).
6. E. J. Takahashi, T. Kanai, Y. Nabekawa, and K. Midorikawa, Appl. Phys. Lett. **93**, 041111 (2008).
7. N. Thiré, S. Beaulieu, V. Cardin, A. Laramée, V. Wanie, B. E. Schmidt, and F. Légaré, Appl. Phys. Lett. **106**, 091110 (2015).
8. V. Cardin, N. Thiré, S. Beaulieu, V. Wanie, F. Légaré, and B. E. Schmidt, Appl. Phys. Lett. **107**, 181101 (2015).
9. B. E. Schmidt, N. Thiré, M. Boivin, A. Laramée, F. Poitras, G. Lebrun, T. Ozaki, H. Ibrahim, and F. Légaré, Nat. Commun. **5**, 3643 (2014).
10. P. Lassonde, N. Thiré, L. Arissian, G. Ernotte, F. Poitras, T. Ozaki, A. Larameé, M. Boivin, H. Ibrahim, F. Légaré, and B. E. Schmidt, IEEE J. Sel. Top. Quantum Electron. **21**, 8700410 (2015).
11. Y. Fu, K. Midorikawa, and E. J. Takahashi, Sci. Rep. **8**, 7692 (2018).
12. Y. Fu, B. Xue, K. Midorikawa, and E. J. Takahashi, Appl. Phys. Lett. **112**, 241105 (2018).
13. X. Gu, G. Marcus, Y. Deng, T. Metzger, C. Teisset, N. Ishii, T. Fuji, A. Baltuska, R. Butkus, V. Pervak, H. Ishizuki, T. Taira, T. Kobayashi, R. Kienberger, and F. Krausz, Opt. Express **17**, 62 (2009).
14. Y. Deng, A. Schwarz, H. Fattahi, M. Ueffing, X. Gu, M. Ossiander, T. Metzger, V. Pervak, H. Ishizuki, T. Taira, T. Kobayashi, G. Marcus, F. Krausz, R. Kienberger, and N. Karpowicz, Opt. Lett. **37**, 4973 (2012).
15. G. Fan, T. Balčiūnas, T. Kanai, T. Flöry, G. Andriukaitis, B. E. Schmidt, F. Légaré, and A. Baltuška, Optica **3**, 1308 (2016).
16. P. Wang, Y. Li, W. Li, H. Su, B. Shao, S. Li, C. Wang, D. Wang, R. Zhao, Y. Peng, Y. Leng, R. Li, and Z. Xu, Opt. Lett. **43**, 2197 (2018).
17. A. Vaupel, N. Bodnar, B. Webb, L. Shah, and M. C. Richardson, Opt. Eng. **53**, 051507 (2014).
18. H. Fattahi, H. G. Barros, M. Gorjan, T. Nubbemeyer, B. Alsaif, C. Y. Teisset, M. Schultze, S. Prinz, M. Haefner, M. Ueffing, A. Alismail, L. Vámos, A. Schwarz, O. Pronin, J. Brons, X. T. Geng, G. Arisholm, M. Ciappina, V. S. Yakovlev, D.-E. Kim, A. M. Azzeer, N. Karpowicz, D. Sutter, Z. Major, T. Metzger, and F. Krausz, Optica **1**, 45 (2014).
19. G. Andriukaitis, T. Balčiūnas, S. Ališauskas, A. Pugžlys, A. Baltuška, T. Popmintchev, M.-C. Chen, M. M. Murnane, and H. C. Kapteyn, Opt. Lett. **36**, 2755 (2011).
20. Y. Yin, J. Li, X. Ren, K. Zhao, Y. Wu, E. Cunningham, and Z. Chang, Opt. Lett. **41**, 1142 (2016).
21. A. V. Mitrofanov, A. A. Voronin, M. V. Rozhko, D. A. Sidorov-Biryukov, A. B. Fedotov, A. Pugžlys, V. Shumakova, S. Ališauskas, A. Baltuška, and A. M. Zheltikov, Optica **4**, 1405 (2017).
22. V. Shumakova, P. Malevich, S. Ališauskas, A. Voronin, A. M. Zheltikov, D. Faccio, D. Kartashov, A. Baltuška, and A. Pugžlys, Nat. Commun. **7**, 12877 (2016).
23. J. Ma, J. Wang, P. Yuan, G. Xie, K. Xiong, Y. Tu, X. Tu, E. Shi, Y. Zheng, and L. Qian, Optica **2**, 1006 (2015).
24. F. Wang, G. Xie, P. Yuan, and L. Qian, Laser Phys. Lett. **12**, 075402 (2015).
25. H. Su, Y. Peng, J. Chen, Y. Li, P. Wang, and Y. Leng, Appl. Sci. **7**, 997 (2017).

https://doi.org/10.1017/hpl.2019.19 Published online by Cambridge University Press